Patient-bounded Extrapolation for 3D Region of Interest Reconstruction in C-arm CT

Yan Xia, Sebastian Bauer, Andreas Maier, Martin Berger, and Joachim Hornegger

***Abstract*—Three-dimensional (3D) region of interest (ROI) imaging with C-arm systems provides anatomical information in a predefined 3D target region at a considerably low X-ray dose. A necessary initial step prior to a 3D acquisition is to isocenter the patient with respect to the target to be scanned. To this end, two low-dose fluoroscopic X-ray acquisitions are usually applied from anterior-posterior (AP) and medio-lateral (ML) views. In this paper, we present a patient-bounded extrapolation method that makes use of these non-collimated fluoroscopic images to improve image quality in 3D ROI reconstruction. The algorithm first extracts the 2D patient contours from the AP and ML images. These 2D contours are then combined to estimate a volumetric model of the patient. Forward-projecting the shape of the model at the eventually acquired C-arm rotation views gives the patient boundary information in the projection domain. In this manner, we are in the position to substantially improve image quality by enforcing the extrapolated line profiles to end at the known patient boundaries, derived from the 3D shape model estimate. The proposed method is evaluated on five clinical datasets with different degrees of truncation. The proposed algorithm achieved a relative root mean square error (rRMSE) of 0.7% with respect to non-truncated data, even in the presence of severe truncation, compared to 8.7% from a state-of-the-art heuristic extrapolation.**

I. Introduction

Three-dimensional (3D) C-arm based region of interest (ROI) tomography that provides anatomical information in a predefined target region at considerably low X-ray dose is a valuable tool in interventional radiology for therapy planning and guidance, particularly for neurointerventions. However, ROI imaging leads to laterally truncated projections from which conventional reconstruction algorithms generally yield images with severe truncation artifacts.

A major category of truncation correction methods is based on estimating the missing data using a heuristic extrapolation procedure, such as symmetric mirroring of projection images (Ohnesorge *et al.* [1]), water cylinder extrapolation (Hsieh *et al.* [2]), square root extrapolation (Sourbelle *et al.* [3]) and hybrid extrapolation (Zellerhoff *et al.* [4]). Although these methods can be carried out without *a priori* information, they rely on heuristics. The degree of accuracy of these extrapolation estimates highly depends on the level of truncation.

Later, Maltz *et al.* [5] observed that the thickness of the patient could be estimated by calculating water-equivalent thicknesses, so that the unknown patient boundary can be approximated. However, in practice, the presence of any non-water tissue may result in a substantial over- or underestimation of the actual object thickness.

Y. Xia, M. Berger, A. Maier and J. Hornegger are with the Pattern Recognition Lab, Friedrich-Alexander-University Erlangen-Nuremberg, Germany. Y. Xia and J. Hornegger are also with the Erlangen Graduate School in Advanced Optical Technologies (SAOT), Germany. S. Bauer is with Siemens AG, Healthcare Sector, Germany.

Disclaimer: The concepts and information presented in this paper are based on research and are not commercially available.

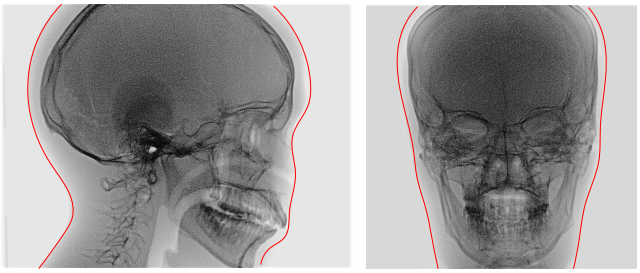

Fig. 1: Illustration of two short fluoroscopic X-ray pulses from ML view (left) and AP view (right), respectively. The red outlines indicate the extracted boundary information.

In contrast, Wiegert *et al.* [6] and Kolditz *et al.* [7] suggested that patient size and shape information can be obtained from an *a priori* low-dose CT scan if available. By forward-projection of this *a priori* CT volume, the collimated regions in the ROI acquisition can be extended in an accurate manner.

In this paper, we present a patient-bounded extrapolation method that leads to major improvements in the quantitative accuracy of 3D ROI imaging, even in the presence of severely truncated data. The method does not require any additional hardware and can be readily integrated into the existing interventional workflow. It is based on the fact that prior to a 3D scan, low-dose fluoroscopic X-ray acquisitions are generally performed from anterior-posterior (AP) and medio-lateral (ML) views, to isocenter the patient with respect to the target to be scanned; see Fig. 1. The fundamental idea of the proposed method is to estimate a 3D shape model of the patient from these low-dose non-truncated fluoroscopic images and then exploit this patient-specific *a priori* shape knowledge for the extrapolation of truncated projections.

II. Method

First, we estimate the rough 3D patient shape based on two low-dose fluoroscopic projections, using per-slice ellipse fitting. The details are elaborated in the following sections; also see Fig. 2 for notations.

Contour-bounded Slice-wise Ellipse Fitting

To extract the boundaries, we first compute the gradient image of fluoroscopic projections and detect the edges using an empirically pre-set threshold. Suppose $\mathbf{u}_{lb}^{AP} = \left(u_{lb}^{AP}, v_i, 1\right)$, $\mathbf{u}_{rb}^{AP}$, $\mathbf{u}_{lb}^{ML}$, and $\mathbf{u}_{rb}^{ML}$ are the homogeneous coordinates of the segmented left and right boundary points at detector row v_i of the 2D fluoroscopic images from AP and ML view. Let $\mathbf{P} \in$

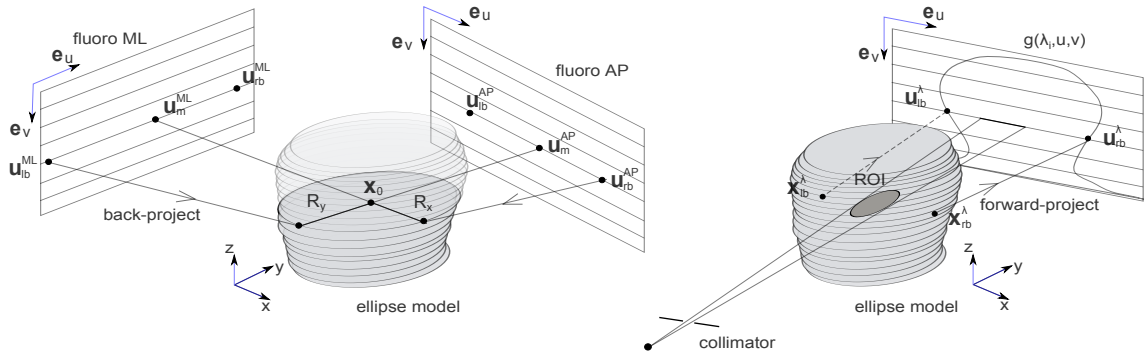

Fig. 2: Illustration of the patient-bounded extrapolation scheme. (Left) Contour-bounded slice-wise ellipse fitting. (Right) Forward-projection of the boundaries of the previously estimated patient shape model at a given C-arm rotation view provides the patient boundary in the projection domain.

$\mathbb{R}^{3\times4}$ be the projection matrix that maps position $\mathbf{x} = [x, y, z]$ in the C-arm coordinate frame to a position $\mathbf{u} = [\omega u, \omega v, \omega]$ in the 2D projection plane:

$$\mathbf{u} = \mathbf{P} \begin{bmatrix} \mathbf{x} \\ 1 \end{bmatrix}. \tag{1}$$

The matrix $\mathbf{P}$ can be decomposed as follows:

$$\mathbf{P} = [\mathbf{P}_{13} \mid \mathbf{p}_4] = [\mathbf{AR} \mid \mathbf{At}] \tag{2}$$

where $\mathbf{R} \in \mathbb{R}^{3\times3}$ denotes the rotation matrix, $\mathbf{t} \in \mathbb{R}^3$ denotes the translation vector, and $\mathbf{A} \in \mathbb{R}^{3\times3}$ the intrinsic parameter matrix.

Then, we can compute the direction unit vector $\boldsymbol{e}_m^{AP}$, $\boldsymbol{e}_m^{ML}$ of the ray that connects the source to the middle point of the two boundaries, i.e., $\mathbf{u}_m^{AP} = \left(\mathbf{u}_{lb}^{AP} + \mathbf{u}_{rb}^{AP}\right)/2$ and $\mathbf{u}_m^{ML} = \left(\mathbf{u}_{lb}^{ML} + \mathbf{u}_{rb}^{ML}\right)/2$, as:

$$\boldsymbol{e}_m^{AP} = \frac{(\mathbf{P}_{13}^{AP})^{-1}\mathbf{u}_m^{AP}}{\|(\mathbf{P}_{13}^{AP})^{-1}\mathbf{u}_m^{AP}\|_2}, \quad \boldsymbol{e}_m^{ML} = \frac{(\mathbf{P}_{13}^{ML})^{-1}\mathbf{u}_m^{ML}}{\|(\mathbf{P}_{13}^{ML})^{-1}\mathbf{u}_m^{ML}\|_2}, \tag{3}$$

where $\mathbf{P}^{-1}$ denotes the pseudo-inverse of the matrix $\mathbf{P}$.

Now the ray equations can be expressed as ($t,\ l \in \mathbb{R}$)

$$\mathbf{l}_m^{AP}(t) = \mathbf{s}^{AP} + t\mathbf{e}_m^{AP}, \text{ and } \mathbf{l}_m^{ML}(l) = \mathbf{s}^{ML} + l\boldsymbol{e}_m^{ML}, \tag{4}$$

where $\mathbf{s}^{AP}$ and $\mathbf{s}^{ML}$ are source positions at AP and ML views, which can be computed using $\mathbf{s} = -\mathbf{P}_{13}^{-1}\mathbf{p}_4$.

Then, the center of the fitted ellipse $\mathbf{x}_0$ is estimated by computing the intersection of the two rays $\mathbf{l}_m^{AP}$ and $\mathbf{l}_m^{ML}$. Here, we confine to breaking the problem down to a 2D line intersecting based on the approximation that $\mathbf{s}^{AP}\mathbf{I}_z = \mathbf{s}^{ML}\mathbf{I}_z$ and $\mathbf{e}_m^{AP}\mathbf{I}_z = \mathbf{e}_m^{ML}\mathbf{I}_z = 0$, where $\mathbf{I}_z = \begin{bmatrix} 0 & 0 & 1 \end{bmatrix}^T$. The third component of $\mathbf{x}_0$ is given by the corresponding slice position. To obtain the intersection point $\mathbf{x}_0$, we establish $\mathbf{s}^{AP} + t\mathbf{e}_m^{AP} = \mathbf{s}^{ML} + l\mathbf{e}_m^{ML}$ and solve for t. Then, substituting t in the first equation of (4) yields:

$$\mathbf{x}_0 = \mathbf{s}^{AP} + \frac{\left\|\left(\mathbf{s}^{ML} - \mathbf{s}^{AP}\right) \times \mathbf{e}_m^{ML}\right\|_2}{\|\mathbf{e}_m^{AP} \times \mathbf{e}_m^{ML}\|_2}\mathbf{e}_m^{AP}. \tag{5}$$

Now we need to determine the radii R_x, R_y of the ellipse. The line equation of the rays from AP view that connects the patient boundary and source can also be expressed as (e.g. right boundary) $\mathbf{l}_r^{AP}(h) = \mathbf{s}^{AP} + h\mathbf{e}_r^{AP}$, where $\mathbf{e}_r^{AP}$ is computed using $\mathbf{u}_{rb}^{AP}$ accordingly. Suppose $\mathbf{x}_r$ is the point

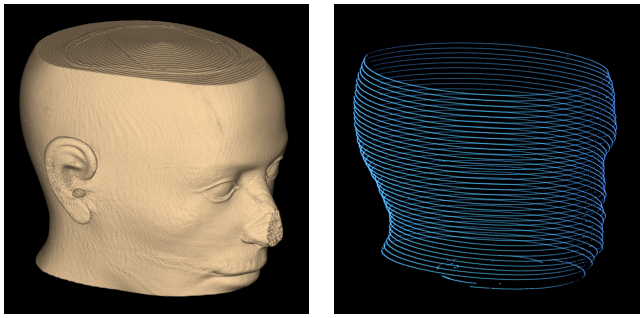

Fig. 3: Visualization of the actual patient shape extracted from a non-collimated 3D reconstruction (left) and the 3D volumetric model estimated from two orthogonal projections with different ellipses in each slice (right).

located on the line $\mathbf{l}_r^{AP}$ that satisfies $\mathbf{x}_r\mathbf{I}_y = \mathbf{x}_0\mathbf{I}_y$, i.e., with the same y-axis coordinate as $\mathbf{x}_0$. Then, the radius along the x-axis R_x can be approximated as follows:

$$R_x = (\mathbf{x}_r - \mathbf{x}_0)\,\mathbf{I}_x \tag{6}$$

where $\mathbf{I}_x = \begin{bmatrix} 1 & 0 & 0 \end{bmatrix}^T$ and $\mathbf{I}_y = \begin{bmatrix} 0 & 1 & 0 \end{bmatrix}^T$.

In analogy, we can use the boundary from ML view to determine the radius of the ellipse along the y-axis R_y.

Patient Boundary Estimation for Arbitrary Angulations

With the estimated ellipse in the volumetric image domain, we can compute the left and right patient boundaries of that ellipse for any given C-arm rotation angle λ as follows:

$$\mathbf{x}_{lb}^{\lambda} = \mathbf{x}_0 - r\mathbf{e}_u, \tag{7}$$

$$\mathbf{x}_{rb}^{\lambda} = \mathbf{x}_0 + r\mathbf{e}_u, \tag{8}$$

where $r = \sqrt{(R_y\cos\lambda)^2 + (R_x\sin\lambda)^2}$ and $\mathbf{e}_u$ denotes the unit vector in detector row direction.

Then, we forward-project these voxel positions to 2D projection plane using Eq. (1), also cf. Fig. 2:

$$\mathbf{u}_{lb}^{\lambda} = \mathbf{P}^{\lambda}\begin{bmatrix} \mathbf{x}_{lb}^{\lambda} \\ 1 \end{bmatrix}, \quad \text{and } \mathbf{u}_{rb}^{\lambda} = \mathbf{P}^{\lambda}\begin{bmatrix} \mathbf{x}_{rb}^{\lambda} \\ 1 \end{bmatrix}. \tag{9}$$

The estimated patient left and right boundaries at the detector row v_i and rotation angle λ, i.e., $\left(u_{lb}^{\lambda}, v_i\right)$ and $\left(u_{rb}^{\lambda}, v_i\right)$, can be easily obtained with $u_{lb}^{\lambda} = \mathbf{u}_{lb}^{\lambda}\mathbf{I}_x / \mathbf{u}_{lb}^{\lambda}\mathbf{I}_z$ and $u_{rb}^{\lambda} = \mathbf{u}_{rb}^{\lambda}\mathbf{I}_x / \mathbf{u}_{rb}^{\lambda}\mathbf{I}_z$.

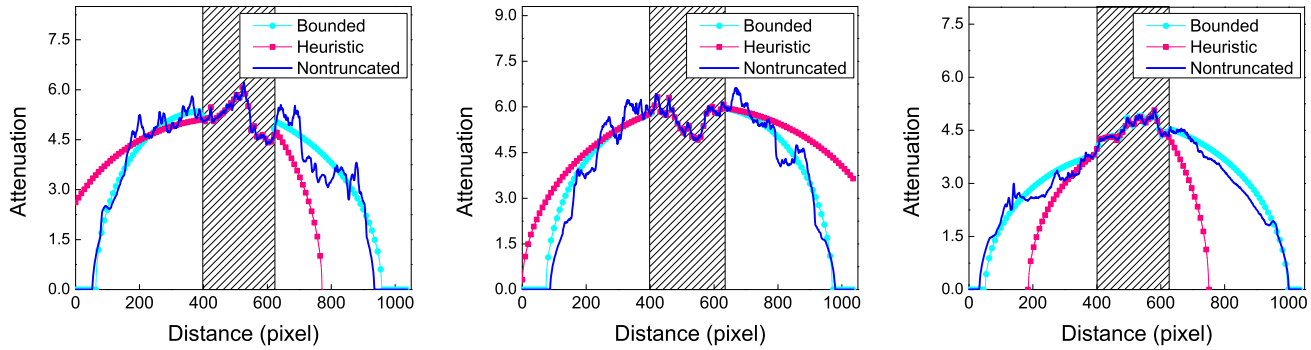

Fig. 4: Comparison of the non-bounded traditional extrapolation and patient-bounded extrapolation in a severe truncation case. Line profiles at projection views of $\lambda = -40°$ (left), $\lambda = 20°$ (middle) and $\lambda = 80°$ (right). Note that the bounded ellipse parameters are estimated using two single projections from $\lambda = -90°$ (ML) and $\lambda = 0°$ (AP). Shaded regions indicate the measured part of projections in ROI scan.

Bounded ROI Projection Profile Extrapolation

Based on the estimated patient boundaries in the ROI scan projection data, we are in the position to apply any extrapolation technique and adapting it according to the restriction that the extrapolated profile must end at the known patient boundaries. In this paper, we adapt the water cylinder approach of Hsieh *et al.* [2] by extending or compressing the initial extrapolated lines to fulfill this restriction. Let $g(\lambda, u, v)$ be the projection data at the detector coordinates (u, v) acquired at angle λ. Then, the extrapolation function is given by

$$\widetilde{g}_{\text{wat}}(\lambda, u, v) = 2\mu\sqrt{R^2 - \xi^2 (u - u_w)^2} \tag{10}$$

where μ is the water attenuation coefficient, u_w is the location of the fitted cylinder with respect to the detector row and R is the radius. The parameters u_w and R are determined as described in [2].

In contrast to the formulation by Hsieh *et al.*, in Eq. (10) we introduce ξ that serves as a scaling factor to stretch or shrink the extrapolated profiles, which is computed as

$$\xi^2 = \frac{R}{u_b - u_w}, \tag{11}$$

where u_b indicates the left or right boundary (u_{lb} or u_{rb}) we obtained in the previous section.

Bounded Square Root Function Extrapolation

As an alternative, we also investigate the square root function extrapolation that was proposed by Sourbelle *et al.* [3]. The extrapolation function is given as

$$\widetilde{g}_{\text{sqr}}(\lambda, u, v) = \sqrt{a \cdot u^2 + b \cdot u + c}. \tag{12}$$

To determine the parameters a, b, and c, the following continuity equations are used:

$$g(\lambda, u_t, v) = \sqrt{a \cdot u_t^2 + b \cdot u_t + c}, \tag{13}$$

$$g'(\lambda, u_t, v) = \frac{b + 2a \cdot u_t}{2g(\lambda, u_t, v)}, \tag{14}$$

where u_t denotes the truncated projection edge and $g'(\lambda, u_t, v)$ is the mean slope value over a small region.

We integrate the patient boundary information into (12) such that the extrapolated profile ends at u_b:

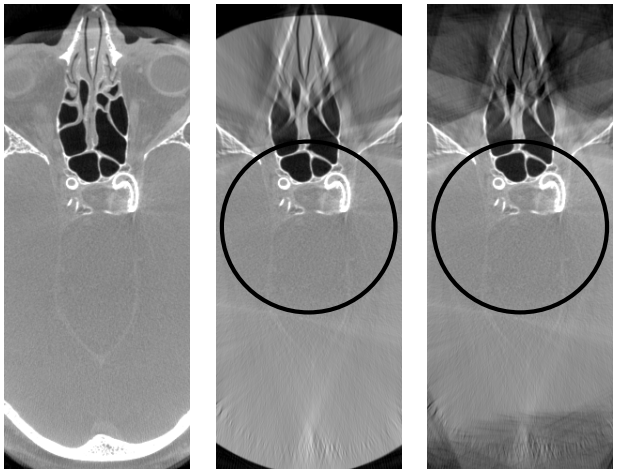

Fig. 5: Transversal slices of the clinical data 1 (medium truncation) reconstructed by FDK from non-truncated data (left), patient-bounded extrapolation (middle), and water cylinder extrapolation (right), in the grayscale window [-1000 HU, 1000 HU]. The black circles indicate the ROI.

$$g(\lambda, u_b, v) = \sqrt{a \cdot u_b^2 + b \cdot u_b + c} = 0. \tag{15}$$

Thus, the three parameters a, b, and c can be determined using these three equations. Note that for both patient bounded extrapolation schemes, we apply a cosine-based smooth weighting on the transition region.

III. Evaluation

A. Experiment Setup

Five clinical datasets of the patients' head (data courtesy of St. Luke's Episcopal Hospital, Houston, TX, USA) were used to evaluate the proposed method. The datasets were acquired on a C-arm system with 496 projection images (1240×960 px) at the resolution of 0.308 mm / px. Even though a practical implementation would involve the extraction of the patient boundaries from low-dose fluoroscopic data, for proof of concept we here confined to extract the boundaries from two projections ($\lambda = -90°$ and $\lambda = 0°$) of a non-collimated 3D scan. All datasets were virtually cropped to a medium field of view (FOV) and a small FOV and were reconstructed onto a volume of 512^3 with an isotropic voxel size of $0.4\,\text{mm}^3$. The

Table I: Quantitative evaluation of truncation corrections for different FOVs. Note that the given RMSE, rRMSE and CC are the average over all five datasets.

	Medium FOV			Small FOV		
	Water cylin. [2]	Bounded water cf. [2]	Bounded sqr. cf. [3]	Water cylin. [2]	Bounded water cf. [2]	Bounded sqr. cf. [3]
RMSE	96.4 HU	30.6 HU	56.1 HU	391.8 HU	43.8 HU	50.6 HU
rRMSE	2.21 %	0.71 %	1.21 %	8.77 %	0.96 %	1.12 %
CC	0.925	0.995	0.992	0.892	0.992	0.991

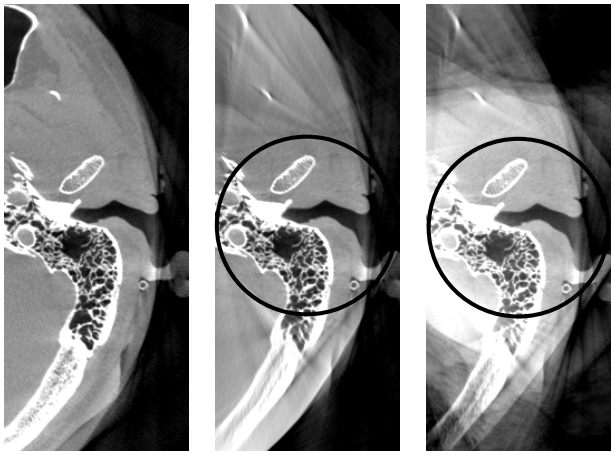

Fig. 6: Transversal slices of the clinical data 2 (off-centered ROI) reconstructed by FDK from non-truncated data (left), patient-bounded extrapolation (middle), and water cylinder extrapolation (right) [-1000 HU, 1000 HU].

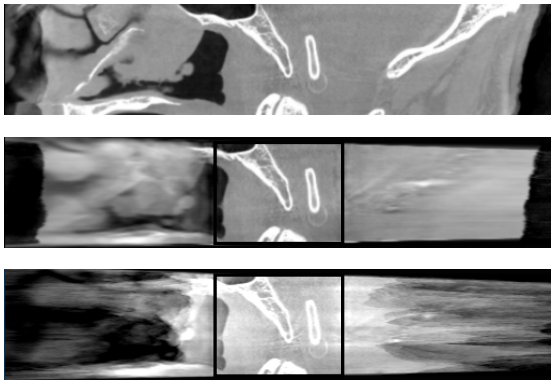

Fig. 7: Sagittal slices of the clinical data 3 (severe trucnation) reconstructed by FDK from non-truncated data (top), patient bounded extrapolation (middle), and water cylinder extrapolation (bottom) [-1000 HU, 1000 HU].

original, non-bounded water cylinder extrapolation (Hsieh *et al.* [2]) was investigated as a baseline and compared to our proposed algorithm for the two schemes. To quantify image quality, three quantitative metrics were used: the root mean square error (RMSE), the relative root mean square error (rRMSE) (i.e., the RMSE divided by the total intensity range) and the correlation coefficient (CC).

B. Results

An example of the estimated ellipse model compared to the actual patient shape extracted from reconstruction is shown in Fig. 3. Figure 4 shows the comparison of the heuristic and proposed extrapolation in a severe truncation case. Reconstruction results from the dataset 1, 2, and 3 are presented in Fig. 5-7, respectively. The quantitative evaluation is summarized in Table I. We can see that the proposed method improves the image quality substantially, particularly for severely truncated data. This is due to the fact that non-bounded heuristic extrapolation can not accurately fit the data outside an ROI, while the proposed method yields a much better approximation; see Fig. 4. The reconstructions also show that the proposed method is robust to both severe truncation and off-centered ROIs. Quantitative accuracy is improved considerably: the average RMSE reached 43.8 HU in severe truncation, compared to 391.8 HU from the heuristic method. A relative error of less than 1% was achieved, yielding an error reduction by a factor of 8 compared the heuristic method.

IV. Discussion

The method we proposed in this paper leads to a major improvement in image quality for 3D C-arm based ROI imaging. It involves no additional radiation when using the fluoroscopic images, as they are acquired anyway during the patient isocentering process. The model estimation can be readily integrated into the existing interventional workflow without additional hardware. Furthermore, it is well-suited for neurointerventions since: 1) The ellipse is a good model for the head; 2) the low-dose fluoroscopic images are usually non-collimated and cover the entire object of interest. Regarding computation times, both slice-wise ellipse fitting and patient boundary estimation are computationally inexpensive since only the boundary points are involved with small vector/matrix multiplications. Due to their very low radiation dose, a sparse set of fluoroscopic images can be further acquired from different views. In this manner, the detailed patient shape could be estimated using some parametric models such as B-splines.

References

[1] B. Ohnesorge, T. Flohr, K. Schwarz, J. P. Heiken, and J. P. Bae, "Efficient correction for CT image artifacts caused by objects extending outside the scan field of view," *Medical Physics*, vol. 27, no. 1, pp. 39–46, 2000.

[2] J. Hsieh, E. Chao, J. Thibault, B. Grekowicz, A. Horst, S. McOlash, and T. J. Myers, "A novel reconstruction algorithm to extend the CT scan field-of-view," *Medical Physics*, vol. 31, no. 9, pp. 2385–2391, 2004.

[3] K. Sourbelle, M. Kachelriess, and W. A. Kalender, "Reconstruction from truncated projections in CT using adaptive detruncation," *European Radiology*, vol. 15, no. 5, pp. 1008–1014, 2005.

[4] B. Zellerhoff, B. Scholz, E. P. Ruehrnschopf, and T. Brunner, "Low contrast 3D-reconstruction from C-arm data," in *Proceedings of SPIE*, 2005, pp. 646–655.

[5] J. D. Maltz, S. Bose, H. P. Shukla, and A. R. Bani-Hashemi, "CT truncation artifact removal using water-equivalent thicknesses derived from truncated projection data," in *IEEE Engineering in Medicine and Biology Society*, 2007, pp. 2905–2911.

[6] J. Wiegert, M. Bertram, T. Netsch, J. Wulff, J. Weese, and G. Rose, "Projection extension for region of interest imaging in cone-beam CT," *Acad. Radiol.*, vol. 12, pp. 1010–23, 2005.

[7] D. Kolditz, Y. Kyriakou, and W. A. Kalender, "Volume-of-interest (VOI) imaging in C-arm flat-detector CT for high image quality at reduced dose," *Medical Physics*, vol. 37, no. 6, pp. 2719–2730, 2010.